Brazilian Journal of Physics (2019) 49:140–150
https://doi.org/10.1007/s13538-018-00629-2

SOCIEDADE BRASILEIRA DE FÍSICA

STATISTICAL

Self-assembly of Droplets in a Straight Microchannel

Erfan Kadivar[1] · **Mojtaba Farrokhbin**[2] · **Fatemeh Ghasemipour**[3]

Received: 23 October 2018 / Published online: 19 December 2018

Abstract

In this work, self-assembly of periodic zigzag arrangement of monodisperse droplets through a flat microfluidic channel is numerically investigated. Our numerical technique is based on the boundary element method (BEM). It is found that droplets having zigzag arrangement tend to travel to channel centerline. We exhibit that non-deformable droplets do not drift normal to the channel centerline. While, as the capillary number increases, deformable droplets tend to approach more to the center of channel and their vertical velocity component increases. Our numerical results illustrate that droplets are dragged by a constant horizontal velocity component which is governed by the continuous phase flow rate. However, this situation is completely different for the vertical velocity component of droplets. We report how the vertical velocity component of droplet towards the channel centerline depends on control parameters such as droplet size, droplet distance, initial configuration, relative orientation of droplets, and capillary number. This dependency plays an important role in estimating necessary time to reach self-assembly.

Keywords Droplet migration · Deformable droplets · Solid particles · Microfluidics · Boundary element method

1 Introduction

Microfluidics is a field which deals with controlling and manipulating fluids in devices where significant lengths are less than a millimeter in size. Fluids behave differently on a micro scale as compared to the macro scale. Interest in microfluidics has been steadily increasing with the availability of many new fabrication techniques which make it possible to invent small devices with great precision and lead to the technological advancements in biotechnology through detection and manipulation on a micron scale. Many disciplines, such as physics, chemistry, and multiple engineering fields have recognized the potential of microfluidics and applied it in their research studies. Nguyen and Wereley [1–5]. Emulsion is a system of two immiscible liquids in which droplet phase is dispersed into continuous phase. Studying the motion of small drops in a viscous fluid is one of the classical problems in fluid mechanics [6–8] and recently attracted many researchers' attention to develop their understanding of the underlying physics behind the droplet motion.

By using the surfactant, the monodisperse emulsions can make themselves more stable in the microfluidic channel. The surfactant solution prevents coalescence of neighboring droplets via repulsive interaction between adsorbed layers on the two colliding drops [9–12]. By using various techniques, droplet motion in the microchannel has been experimentally and numerically investigated [13–16]. The path of produced droplet is a function of channel geometry, droplet size, position of other produced droplets, and physicochemical parameters [17–20].

A wide range of experimental techniques has been used to produce one or two-row zigzag pattern of droplets in the microchannels [21–24]. The transition between single-row and two-row packings [25–27], and also collective modes of monodisperse droplets have been studied [28, 29]. The theoretical and experimental studies of droplet migration towards the centerline of flow indicate a shear-induced dispersion due to droplet-droplet interaction [30, 31]. The droplet-droplet interaction has an important role in establishing a steady-state distribution [32–34]. The experimental observations indicate that

✉ Erfan Kadivar
erfan.kadivar@sutech.ac.ir

[1] Department of Physics, Shiraz University of Technology, Shiraz, 71555-313, Iran

[2] Department of Physics, Faculty of Sciences, Yazd University, Yazd, 89195-741, Iran

[3] Department of Physics, Shahid Beheshti University, G.C., Evin, Tehran, 19839, Iran

initial lateral perturbation results an instability in trailing drops [28]. However, rigid spheres and deformable drops display different collective dynamics. Deformable drops are stabilized into drop arrays due to their tendency towards aligning in the flow direction [33] while a linear array of rigid spheres exhibit particles pairing instability in the flow direction. The dipolar hydrodynamic interactions impose macroscopic phenomena which are affected by particle size and deformability. The shear flow exerted by channel wall drives droplets to migrate towards the centerline of channel.

In this work, we present a numerical study on the self-assembly of two-row arrangement of two-dimensional monodisperse droplets (disk-like droplets) flowing through a flat straight microfluidic channel. Here, we assume that channel width-to-depth ratio is large compared to one. Therefore, instead of solving three-dimensional problem, we solve a depth-averaged problem. Hence, we consider two-dimensional flow of both liquids which can be governed by Darcy equation. According to the considered periodic pattern, we divide channel length into periodic boxes. The two-dimensional Darcy flow will be numerically solved in one periodic box. The solution of depth-averaged Darcy equation is numerically obtained via a self-consistent integral equation using the boundary element method (BEM). Therefore, we calculate the pressure and velocity at droplet-continuous interface. In this study, we investigate the transition between two-row and two-row arrangements of disk-like droplets flowing through the microchannel. As a much more important application, we discuss how relationships between droplets velocity and control parameters such as droplet size, flow rate, viscosity, and capillary number towards reaching the self-assembly. These relationships play an important role to obtain necessary time to reach the self-assembly of the system. Finally, we investigate the effect of droplet deformability on the drift velocity of droplets normal to the channel centerline.

This paper is structured as follows: In the following Section 2, we will formulate Darcy equation and boundary conditions for the velocity field of quasi-two-dimensional droplets in a flat microfluidic channel. The numerical procedure to solve the integral equation of pressure field and, thus, the droplets motion are also contained in Section 2. The results of our numerical solutions, including the velocity dependency of droplets to control parameters are reported in Section 3. In Section 3, we will investigate the effect of droplet size, droplet-droplet distance, viscosity ratio, and capillary number on the droplet migration towards the channel center. Finally, we summarize our findings and conclude in Section 4.

2 Governing Equations

In this work, we numerically study the dynamics of monodisperse emulsion droplets flowing in the flat microfluidic channel. We consider a periodic array of droplets which flow with offset to the top and bottom of flat microfluidic channel centerline. The droplet phase and continuous phase are labeled by d and c, respectively. The channel length is along the x-axis and width of the channel is along the y-axis. The channel height, H, is assumed to be much smaller than the channel width, W, and droplet radius, R_d. Therefore, droplets are confined between the top and bottom walls of the microchannel. Hence, droplets flowing through the microchannel possess disk-shape (pancake shape) which is called disk-like droplets.

Due to the small length scale, flow rate usually ranges between a few nl/min to $\mu l/min$ and the Reynolds number is small. In this limit, fluidic resistance in the microfluidic channel is high. Experimental observations indicate that at thin channels, the velocity profile in the direction of channel thickness, z-axis, is assumed to be parabolic. However, far from the walls, it is almost constant along the y-axis. It is easy to verify that by increasing the aspect ratio of channel width to channel height, the velocity field computed from the 3D Stokes equation in the x-y plane and far from the walls tends to constant value in the y-direction. Therefore, instead of solving the 3D Stokes equation, we solve a depth-averaged problem which is labeled two-dimensional problem. This flow can be well approximated by a two-dimensional description. Such two-dimensional flow in a Hele-Shaw cell obeys Darcy's law; this laminar flow is mathematically equivalent to flow in a porous medium [35, 36].

In the Hele-Shaw limit, the flow velocity obeys locally a Poiseuille profile $(u_x, u_y, u_z) = 3/2(1 - 4z^2/H^2)\,(\bar{u}_x, \bar{u}_y, 0)$. Deviations from the Poiseuille profile become apparent once the distance to the side walls becomes the order of cell height, H, or smaller. In this work, the depth averaged velocity $\boldsymbol{u} = (\bar{u}_x, \bar{u}_y)$ for both droplet and continuous phase are applied. Under this assumption, when gravitational force is negligible, the velocity field inside and outside of droplet are governed by continuity equation

$$\nabla.\boldsymbol{u}_i = 0 \qquad \text{on} \quad \Omega_i \quad \text{with} \quad i \in \{\text{c}, \text{d}\}\,, \tag{1}$$

and the Darcy equation [35]

$$\boldsymbol{u}_i = -\alpha_i \nabla P_i \qquad \text{on} \quad \Omega_i \quad \text{with} \quad i \in \{\text{c}, \text{d}\}\,, \tag{2}$$

where $\nabla = (\partial_x, \partial_y)$ is the two-dimensional Nabla operator, $P(x, y)$ is the pressure, and $\boldsymbol{u}$ is the velocity. $\alpha_i = \frac{H^2}{12\mu_i}$ is the liquid mobility and μ is the viscosity.

Evolution of the droplet interface is governed by mass conservation. If there is no mass transfer through the interface, kinematic boundary condition at the droplet-continuous phase interface imposes the continuity of the normal velocity component. This boundary condition reads

$$\mathbf{n}\cdot\boldsymbol{u}_c=\mathbf{n}\cdot\boldsymbol{u}_d\neq 0 \qquad \text{on} \qquad \Gamma_{\mathrm{cd}}\,, \tag{3}$$

where unit normal vector, $\mathbf{n}$, points from the interior of the droplet phase into the continuous phase and Γ_{cd} is the two-dimensional droplet contour.

An other droplet interface condition is discontinuity of normal stress due to surface tension, γ, and curvature. The two principal curvatures are an in-plane curvature $K_{\parallel}$ and a meniscus curvature in the thin direction, $K_{\perp}$. In flat channels, i.e., where the ratio of channel width to channel height is large compared to one, droplet adopts the disk-like shape. In this case, the radius of curvature of the free in-plane droplet contour, i.e., the parts of the contour that are not in contact with either the channel wall or another droplet, will be much larger than the height of the channel. The mean curvature, K_m, of the liquid-liquid interface reads [37]

$$K_m=K_{\perp}+\nu K_{\parallel} \tag{4}$$

where the out-of-plane curvature of the liquid-liquid interface, $K_{\perp}$, can be approximated by $2/H$ and the in-plane curvature of the droplet contour $K_{\parallel}=1/R_d$. The numerical prefactor, ν is not identical to one. In accordance with real droplet microfluidic system, one assumes a non-wetting dispersed phase, the value of $\pi/4$ for perfectly non-wetting conditions was derived by Park and Homsy [37]. The prefactor of $\pi/4$ can be understood from the limiting process mapping a three-dimensional droplet to the purely two-dimensional model. Throughout this work, we have assumed perfectly non-wetting condition for the dispersed phase on the channel walls, which is the usual case in droplet-based microfluidic, where surfactant is used to prevent the merging of droplets. Therefore, a relation between the mean local curvature, K_m, and interfacial tension, γ, of the liquid-liquid interface to the difference between the pressure inside the droplet phase, P_{d}, and the pressure in the continuous phase, P_{c}, at each point of the droplet contour is given by a two-dimensional analogue of the Laplace's law [37]:

$$P_{\mathrm{c}}-P_{\mathrm{d}}=\frac{\pi}{4}\,\gamma\,K_m\,. \tag{5}$$

On the channel walls, because of the impermeability of the channel side walls Γ_w, we have

$$\mathbf{n}_w\cdot\nabla P_c=0 \qquad \text{on} \qquad \Gamma_{\mathrm{w}}\,, \tag{6}$$

where the normal vector $\mathbf{n}_w$ on Γ_{w} points from the inside of the wall into the continuous phase.

Employing the continuity equation, the pressure in the dispersed and the continuous phase satisfy the Laplace equation

$$\nabla^2 P_i=0 \qquad \text{on} \quad \Omega_i \quad \text{with} \quad i\in\{\mathrm{c},\mathrm{d}\}\,, \tag{7}$$

To evolve the droplet interface under flowing in time, we calculate the normal component, $\mathbf{n}\cdot\boldsymbol{u}$, of the local depth averaged velocity at the droplet contour. Solutions to (7) for appropriate boundary conditions (3), (5), (6) together with the Darcy (2) describe the velocity field of the liquid in the dispersed and continuous phase. In this way, we need to obtain the relevant boundary data of the velocity field. A self-consistent integral equation which links the pressure field P_{c} of the continuous phase on the boundary $\Gamma_{\mathrm{d}}\cap\Gamma_{\mathrm{w}}$ to its normal derivative $\mathbf{n}\cdot\nabla P_{\mathrm{c}}$ should be solved. Following the formulation of Pozrikidis [38], the pressure field of the continuous phase has to obey an integral equation of the explicit form [40]

$$\begin{aligned}P_{\mathrm{c}}(\mathbf{r}_0)=&\int_{\Gamma_{\mathrm{w}}}P_{\mathrm{c}}\mathbf{n}_w\cdot\nabla G(\mathbf{r},\mathbf{r}_0)\mathrm{d}\ell-\int_{\Gamma_w}G(\mathbf{r},\mathbf{r}_0)\mathbf{n}_w\cdot\nabla P_c\mathrm{d}\ell\\&-\int_{\Gamma_{\mathrm{cd}}}\left\{\frac{\pi}{4}\alpha_{\mathrm{r}}\,\gamma\,K_m\,\mathbf{n}\cdot\nabla G(\mathbf{r},\mathbf{r}_0)-(1-\alpha_{\mathrm{r}})\,P_{\mathrm{c}}\mathbf{n}\cdot\nabla G(\mathbf{r},\mathbf{r}_0)\right\}\mathrm{d}\ell,\end{aligned} \tag{8}$$

where $\mathbf{r}=(x,y)$ is field point, $\mathbf{r}_0=(x_0,y_0)$ is singular point on the boundary $\Gamma_{\mathrm{cd}}\cap\Gamma_{\mathrm{w}}$ of the continuous phase, and $\alpha_{\mathrm{r}}=\alpha_d/\alpha_c$ is the mobility ratio of droplet phase to continuous phase. In the case of non-periodic flow, the integration contour in above equation, Γ_{w}, is the channel boundaries; for flow in free space, $G(\mathbf{r},\mathbf{r}_0)$ represents the harmonic potential at the point $\mathbf{r}$ due to a point sink of unit strength located at the point $\mathbf{r}_0$, given by $G(\mathbf{r},\mathbf{r_0})=-\frac{1}{2\pi}\ln|\mathbf{r}-\mathbf{r_0}|$. In the case of singly periodic flow, Γ_{w} is enclosed by one period of the flow; for flow in free space, $G(\mathbf{r},\mathbf{r}_0)$ represents the flow due to a one-dimensional array of point sinks of unit strength, one of which is located at the point $\mathbf{r}_0$. The periodic Green's function in free space represents the flow due to an infinite periodic array of point forces separated by the distance L along the x axis, is given by [38]

$$G(\mathbf{r},\mathbf{r_0})=-\frac{1}{4\pi}\ln[2\{\cosh[k(y-y_0)]-\cos[k(x-x_0)]\}]\,, \tag{9}$$

where $k=2\pi/L_{PB}$ is the wave number, and L_{PB} is the periodic length.

Figure 1 illustrates the initial configuration of two-row zigzag arrangement of droplets flowing through the microchannel. As can be seen in Fig. 1, the microchannel walls are located at $y=-W/2$ and $W/2$, where W is the channel width. According to the periodic structure of droplets in the channel, we divide channel space into periodic boxes [27, 39]. We solve the Darcy (2) in one periodic box. In this way, we consider two droplets in one

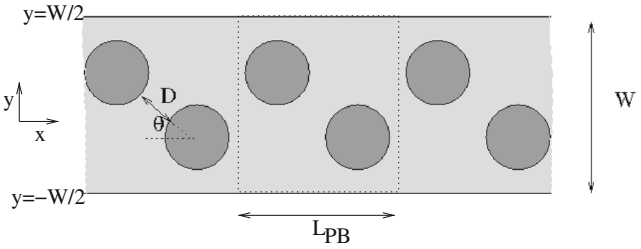

Fig. 1 Top view of two-row zigzag arrangement of pancake-like droplets flowing through the flat microfluidic channel. The continuous phase drags the droplets towards the right. To have the symmetrically pattern, we choose origin of the coordinate at the center of the channel. L_{PB} is the length of periodic unit box. It is clear that L_{PB} depends on the droplet size, and droplet configuration

periodic simulation box. Depending on droplet size, each droplet in periodic box has two or four closest neighbors. L_{PB} is the box length of the 2D periodic box (see Fig. 1). The size and shape of periodic box are updated as the droplets flow through the channel. Hence, the length of periodic box, L_{PB}, depends on time, droplet size, relative orientation of droplets, θ, and interface-interface droplets separation distance, D.

We decompose the pressure into two terms: $P_c^{(b)}$ the pressure along the channel in the absence of droplets, and the disturbance part of pressure due to the presence of droplets at one periodic box, $P_c^{(d)}$.

$$P_c = P_c^{(b)} + P_c^{(d)} \ . \tag{10}$$

According to Darcy equation, in the absence of droplet, there is a linear relation between the pressure of bare continuous phase and channel length:

$$P_c^{(b)} = -\alpha_c u_0 x + \text{constant} \ , \tag{11}$$

where u_0 is the constant velocity of continuous phase in the absence of droplets.

To solve the self-consistent integral equation, we define non-dimensionalized physical quantities. To this end, we have chosen suitable length scale L_0, time scale T_0, and pressure scale p_0, and have expressed physical quantities in terms of these three basic units. As our unit length, we have chosen length scale $L_0 \equiv W$, time scale $T_0 \equiv \mu_c W/\gamma$, pressure scale $p_0 \equiv \gamma/W$, and Capillary number $\text{Ca} = \mu_c u_0/\gamma$. When expressing all relevant physical quantities in these units, the viscosity of the continuous phase μ_c, and the channel width W all equal unity. Hence, the dimensionless droplet area, a, is defined as the droplet area divided by the squared channel width, $a = \pi R_d^2/W^2$. Here, and in the remainder of this article, we will denote all non-dimensional rescaled lengths and physical quantities by lower case symbols.

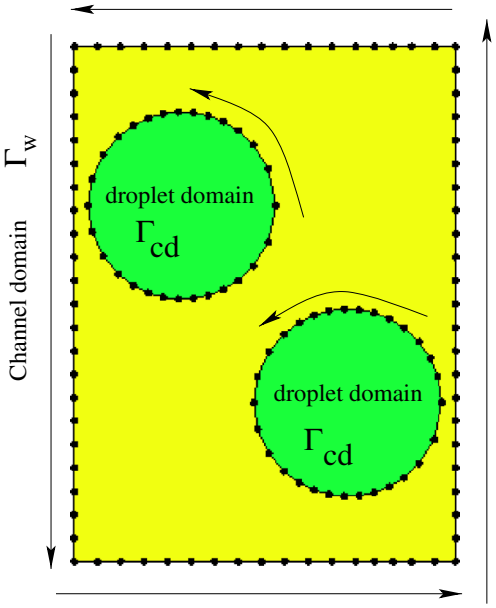

Fig. 2 Boundary element mesh for the droplets and continuous phase. Arrows illustrate the boundary integral paths. The self-integral is solved in a periodic box. The length of periodic box is L_{PB}. Γ_{cd} and Γ_w are the two-dimensional droplet and channel contours, respectively

2.1 Boundary Discretization

Boundary discretization is the first step towards solving the self-consistent integral equation. There are a variety of boundary elements in two dimensions. Since the boundary element method is only implemented for boundaries, it is unnecessary to mesh the whole domain. In this way, the discretization of droplet-continuous phase interface into a collection of N elements has been performed by cubic-spline method. The advantage of this method is that the slope and curvature at the end point of elements are smooth. Because the droplet is closed surface, we have applied periodicity conditions for the first and second derivative at the first and last nodes. In contrast to the droplet contours, the channel walls are not interpolated by cubic splines and given by straight segments. Figure 2 illustrates that how the continuous and droplet domains are coupled. The boundary integration is performed counter-clockwise around a domain. Arrows present the boundary integral paths. The mesh independence has been verified by calculating the droplet area as function of time. According to continuity equation, it is clear that the droplet area must be constant over the time. It was found that 200 points for droplets contour and 150 straight elements for fixed

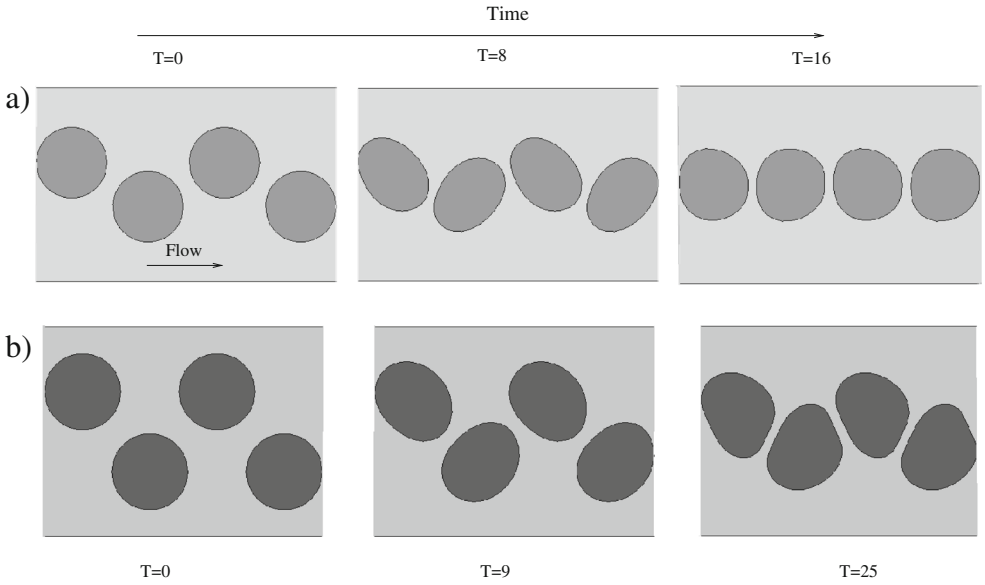

Fig. 3 Snapshots of a train of droplets in the flat microfluidic channel at different times. As time goes, droplets drift normal to channel walls in the considered zigzag arrangement. Numerical parameters are as follows: **a** droplet size $a = 0.103$, $D = 0.901$, $\theta = 30°$, and $Ca = 0.23$; **b** $a = 0.103$, $D = 0.136$, $\theta = 55°$, and $Ca = 0.23$

boundaries are satisfactory and any increase beyond this mesh size would lead to insignificant changes in the results.

The boundary integral (8) is discretized with a collection method and integrated by $Gauss - Legendre$ quadrature with 12 nodes. Therefore, we calculate the pressure and velocity at the collection points. After that, we update the position of the points by using an explicit Euler method. Using the explicit Euler, the interface droplet is advanced in discrete time step. Since the points change their relative positions on Γ_{cd} with time, it is necessary to remesh the splines at each time step. When the relative position of two adjacent nodes on the interface is twice as big or twice as small as the initial size, the points are remeshed equidistantly using a cubic interpolation [40].

3 Results

In this work, we investigate fundamental mechanism of droplets motion, velocity dependence, and explore their limitations in practical applications. In this way, we consider initial configuration of two-row zigzag arrangement of pancake-like droplets flowing through the microfluidic channel (see Fig. 1). As shown in Fig. 1, the interface-interface separation distance is called, D, and relative orientation of droplets is labeled by θ which is an angle between D and x-axis. Through our numerical setup, $\theta = 0$ corresponds to the case that all droplets flow on one line which lies in the centerline of channel, while $\theta = 90$ illustrates that droplet are exactly located on top of each other. The channel width characterized by the uniform width W. In dimensionless scale, the length scale $L_0 = W = 1$ and the channel length is fixed by 100 times the channel width and the aspect ratio of channel width to channel height is 8, $W/H = 8$. The continuous fluid is injected from the left side.

We consider the initial configuration of zigzag arrangement of droplets in the flat channel. By flowing the droplets through the channel, the motion of droplets perturbs the flow of the continuous phase. This perturbation affects the motion of other droplets in the microfluidic channel. Therefore, the droplets tend to flow to the centerline of the channel (see Supplementary Information, Movie). This property is a direct result of the velocity profile of continuous phase in the presence of droplets (pressure gradient along the y-axis). Figure 3 illustrates the snapshots of a train of two-row zigzag arrangement of droplets in the flat microfluidic channel. Our numerical results indicate that, when the interface-interface separation distance is too large with respect to the droplet diameter, the droplets reach the channel centerline and they finally travel on the centerline of channel. Figure 3a presents a continuous transition between two-row zigzag structure to one-row structure. As one can see in Fig. 3a, by passing time, the droplets drift normal to the channel walls and the finally flow on the channel centerline. An other regime has been observed in our numerical simulation is that by passing the time, droplets migrate to centerline of channel, but they cannot reach the centerline and final arrangement is two zigzag configuration (see Fig. 3b). Our numerical observations indicate that the final arrangement depends on the droplet size, a, interface-interface droplet distance, D, and relative orientation of droplets, θ.

Figure 4 illustrates the x- and y-position of droplets flowing through a straight channel as a function of time

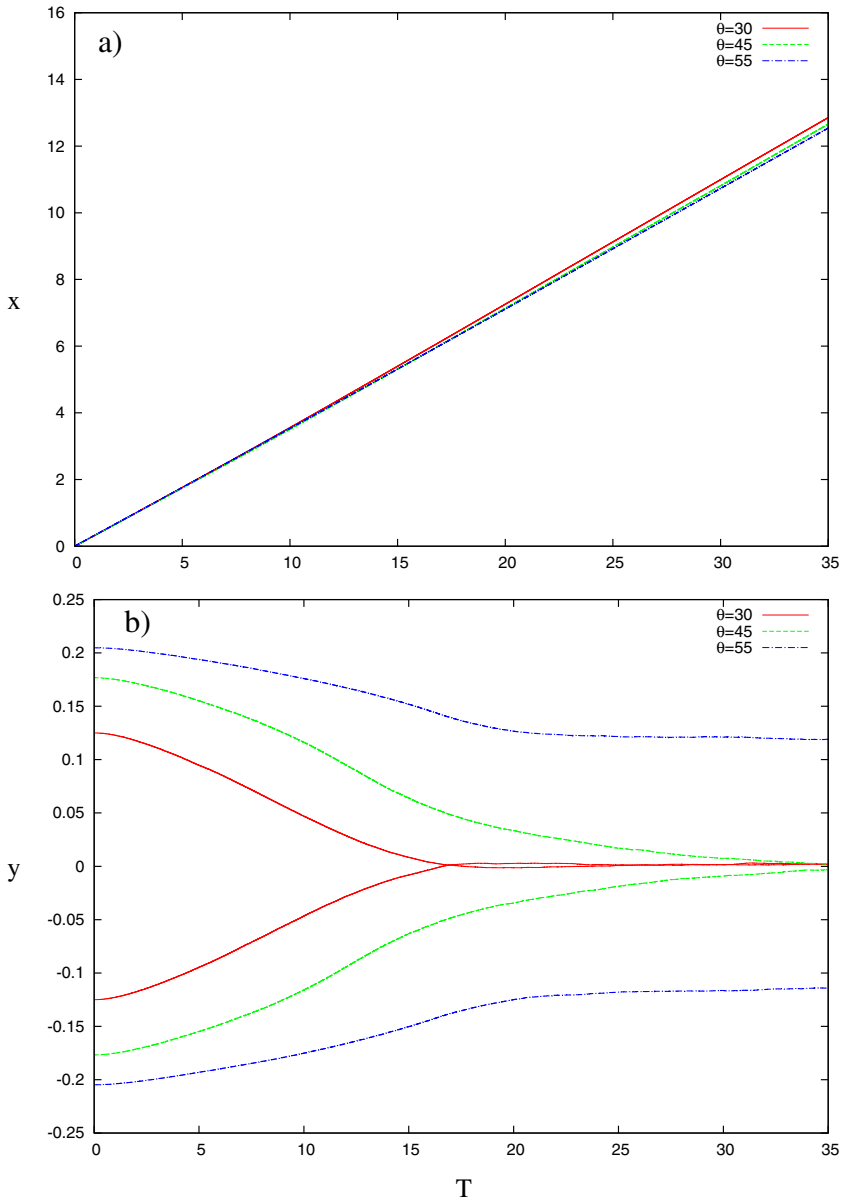

Fig. 4 **a** Numerical graph of x-position of droplets trajectory as a function of dimensionless time for different values of θ. **b** y-normalized position of droplets trajectory versus dimensionless time. According to periodic symmetry of droplets arrangement, the channel domain is divided to periodic boxes which contain two droplets in each box. A detailed description is given in the main text. The horizontal and vertical velocities of droplets are calculated using the position-time curve. Numerical parameters are as follows: $D = 0.136$, and $a = 0.103$

for given value of droplet size. We evaluate x- and y- components of average drift velocity (u_x^D, u_y^D) by using position-time plots. The average droplet velocity is calculated from the initial position to relaxed point where y-position is fixed (see Fig. 4). Figure 4a shows the x-component graph of droplet displacement versus time for different values of θ. It can be seen that the graph consists of straight lines. Our numerical results indicate that x-component of droplets velocity, u_x^D, is fixed by the flow rate of the continuous phase and it is independent of droplet size and droplet arrangement, θ. Figure 4b illustrates the y-positions of two droplets traveling through a straight channel as a function of dimensionless time for different values of θ. Figure 4b demonstrates that the droplets tend to move to the center of channel. However, the averaged vertical velocity component of droplets, u_y^D, strongly depends on the control parameters such as droplet size, droplet distance, initial configuration, relative orientation of droplets, and capillary number.

The solid curves in Fig. 4b illustrate that the droplets migrate towards channel centerline and finally they reach it. By increasing the θ, they cannot flow on the centerline on channel. It means that for given value of droplet size, a, and droplet distance, D, there is a critical value of θ_c, at which two-row to one-row transition does not occur. Figure 5

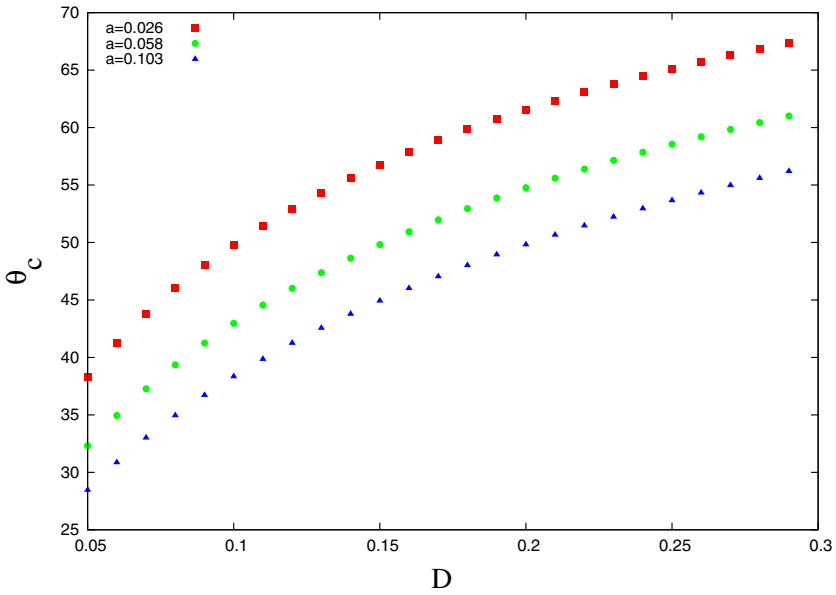

Fig. 5 Critical relative orientation of droplets, θ_c as function of interface-interface separation distance, D, for different values of droplet size

presents the behavior of θ_c as a function of droplet distance for three values of droplet size.

Our numerical findings indicate that the droplet migration mechanism towards the channel center is strongly dependent on initial configuration of droplets, droplet size, viscosity ratio, and capillary number. In this work, we investigate and discuss the influence relative orientation of droplets, droplet size, viscosity ratio, and capillary number on the drift velocity component of droplet normal to the channel centerline.

3.1 Validation: Comparison with Experiments

To validate the consistency of the numerical model, we compare our numerical data and shape with available experimental data and images. At first, we use the experimental image of Mehrotra et al. [41] to demonstrate the validity of our numerical snapshots. Figure 6 illustrates the microscopic images of droplets trajectory in the straight microchannel. As one can see, droplets tend to travel to the center of the channel. The image on the left was taken at cross junction point A and the image on the right was taken at detection point C (1 cm from the cross junction) [41]. Now, we compare the trajectory reported by Karin and Mason experimental observations [42] with the simulated ones which were obtained using the same conditions of flow rate and droplet size. Simulation and experiment results seem to be in good quantitative agreement, as shown in Fig. 7.

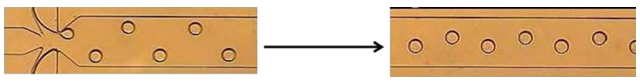

Fig. 6 Experimental images of droplets trajectory in microfluidic channel reported in Ref. [41]

3.2 Effect of Relative Orientation of Droplets

First, we investigate the effect of relative orientation of droplets on the vertical component of droplet velocity. Figure 8 illustrates the vertical component of the droplet velocity as a function of the relative orientation of droplets, θ, for given droplet size (see Fig.1). Numerical results show that u_y^D first increases monotonically from zero (for the case that droplets are flowing on center line of channel) to its maximum value at θ_m. About θ_m, the change in velocity is not affected so much. Above θ_m, falling in u_y^D becomes steep. Moreover, it is clear to see that, at given value of θ, closer droplets have steeper slope in u_y^D. Therefore, the vertical velocity of droplets depends on the initial relative orientation of droplets, θ, and droplet-droplet distance, D (see Fig. 8 for more details). The maximum value also strongly depends on the droplet distance and droplet size.

3.3 Effect of Droplet Size

Figure 9 presents the behavior of vertical velocity for different droplet sizes at given value of droplet distance. Numerical results indicate that the vertical component of velocity strongly depends on the droplet size and θ. This result comes from this physical fact that the droplet motion in periodic box perturbs the flow of continuous phase. This perturbation is a function of droplet size. When the droplet distance being kept constant, by increasing the droplet size, the vertical component of droplet velocity increases. The motion of droplets result in symmetry breaking flow and

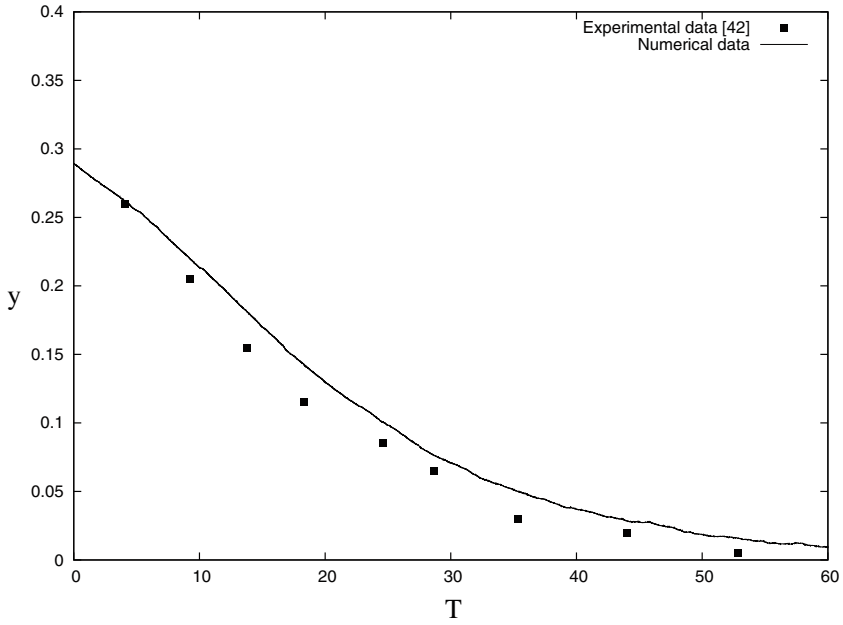

Fig. 7 Migration of droplets towards the centerline of microchannel. y-normalized position of droplet trajectory versus dimensionless time. Black solid squares are extracted from the experimental data [42] and black solid line corresponds to our simulations

induce dipolar flow fields, which bring $\frac{1}{r^2}$ hydrodynamic interaction between the droplets [28, 29]. Therefore, long-range hydrodynamic dipolar interaction attract droplets to each other and align them along the centerline of channel. This leads the zigzag pattern turns to the droplets flowing in a straight centerline.

3.4 Effect of Viscosity Ratio

In order to quantify the dependence of the y-component of droplet velocity on viscosity ratio, we fix droplet size and droplet-droplet distance. The velocity of continuous phase depends on the continuous phase viscosity. Therefore, we keep the continuous phase viscosity and vary the viscosity of droplet phase. Figure 10 illustrates the effect of dispersed- to continuous-phase viscosity ratio on the y-component of droplet velocity. According to Darcy equation, the droplet velocity is proportional to the inverse of viscosity. Therefore, as the viscosity ratio decreases, the vertical velocity component of droplet increases. As one can see in Fig. 10, at given value of capillary number, the y-component of droplet velocity increases by decreasing the viscosity ratio. For larger capillary number, increasing in vertical velocity will be more steeper.

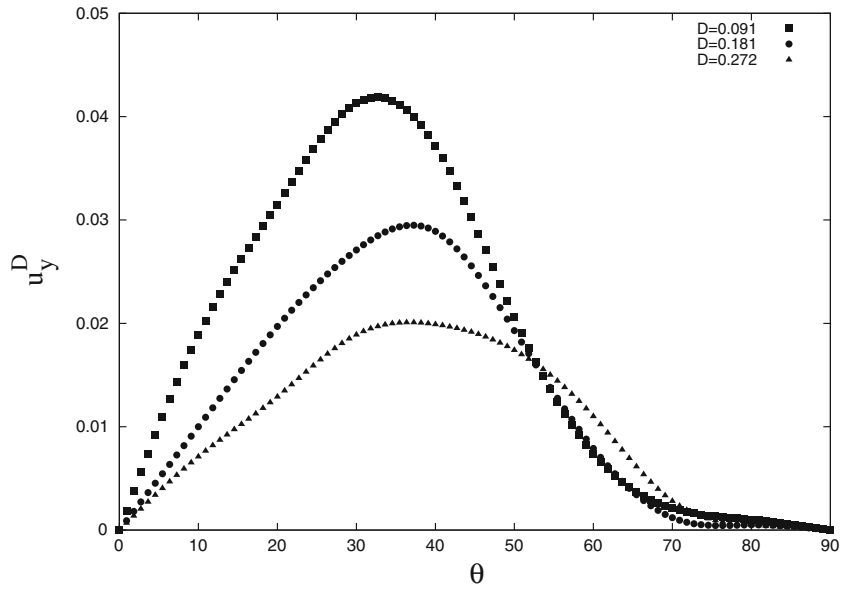

Fig. 8 vertical component of droplet velocity as function of θ for different interface-interface separation distance of droplets, D, and given value of droplet size, $a = 0.103$

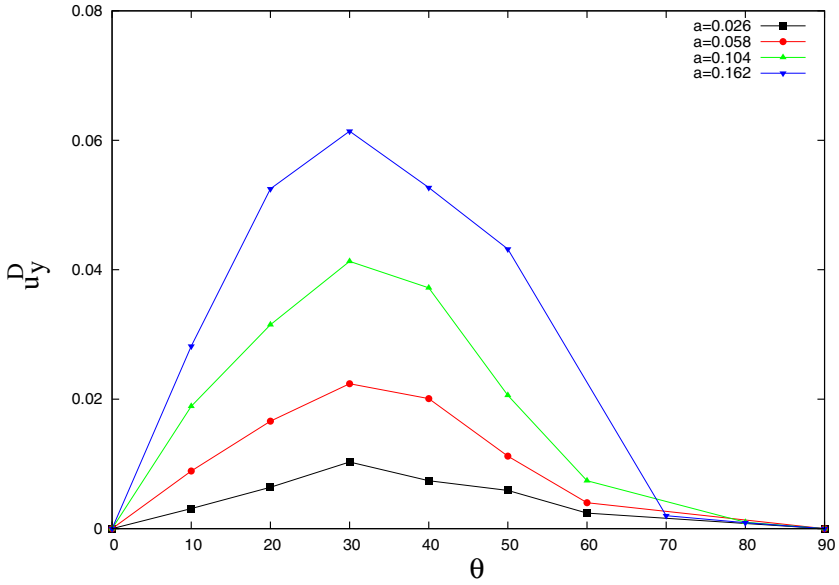

Fig. 9 y-component of droplet velocity, u_y^D as a function of θ for different droplet size , a, and given value of droplet distance, $D = 0.091$. The lines are drawn only to guide eyes

3.5 Effect of Capillary Number

In order to understand more the effect of droplet deformability on droplet migration, we fix droplet size and vary the surface tension. To present our numerical result in dimensionless unit, we have used the capillary number. The droplet deformation increases with increasing the capillary number at constant viscosity ratio. Figure 11 illustrates the vertical velocity component of droplets as function of capillary number. Our numerical results indicate that the vertical velocity component increases as the capillary number increases. Indeed, the droplet deformability has an important role in the drift velocity. Both nondeformable and deformable particles immersed in a continuous phase produce a disturbance velocity. In solid particle case, the disturbance velocity is symmetric and solid particles do not drift normal to channel (see low values of capillary number in Fig. 11). However, the disturbance velocity of deformable droplets is asymmetric. This inhomogeneity of droplet velocity in the normal direction creates an additional non-zero mean value of normal velocity component. Therefore, a deformable droplet in Darcy flow drifts towards the centerline of channel where shear stress is minimized. Since the shear stress is minimum at the center of the channel and maximum at the channel walls, this pressure difference across the channel width specifies the path of the droplets.

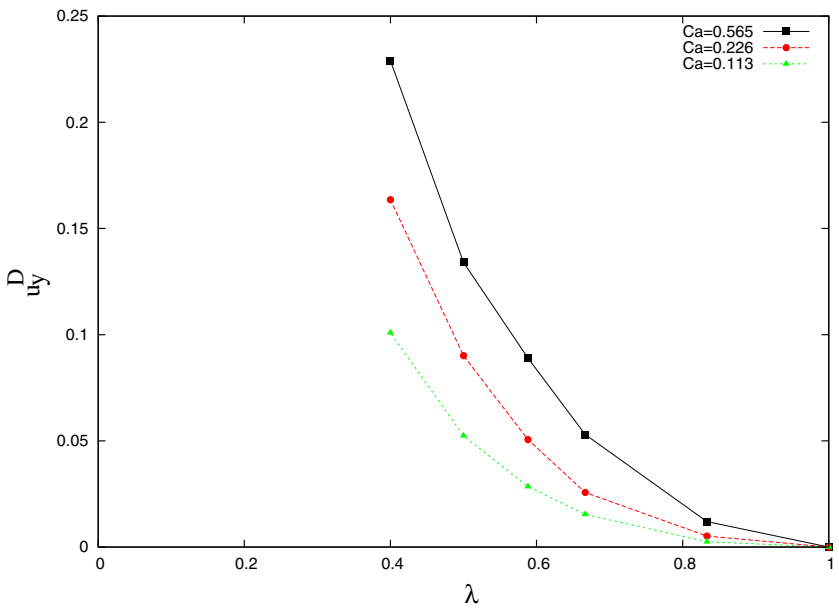

Fig. 10 Vertical component of droplet velocity as a function of viscosity ratio λ for three different values of capillary number. The lines are drawn only to guide eyes. Numerical data are droplet size , $a = 0.103$, $D = 0.125$, and $\theta = 22°$

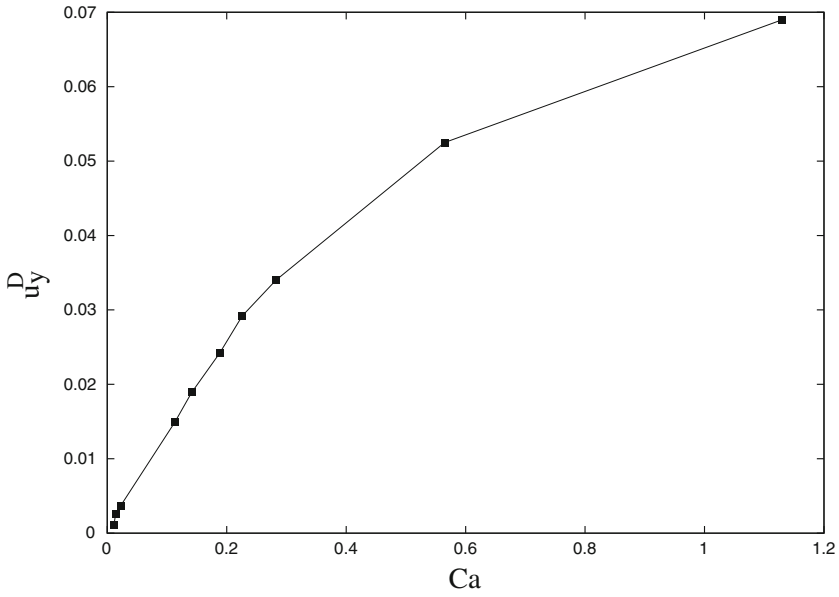

Fig. 11 vertical component of droplet velocity as a function of capillary number Ca. The solid line is drawn only to guide eyes. Numerical data are droplet size, $a = 0.103$, $D = 0.125$, $\lambda = 0.67$, and $\theta = 22^\circ$

4 Conclusion

In this work, the velocity dependence of a periodic zigzag arrangement of monodisperse disk-like droplets in a flat microfluidic channel has been studied. Previous studies have been based on phenomenological and experimental models to investigate the packing configuration or collective modes. By assuming quasi-two-dimensional flow, we numerically solved the two-dimensional Darcy flow through periodic array of disk-like droplets in a flat microfluidic channel employing the boundary element method (BEM). We have divided the channel space into periodic boxes to tackle the simulation of periodic system. In what follows, two droplets have been considered in one simulation box.

Our numerical results illustrate that the droplets tend to travel to the center of the channel where minimum pressure is created by the continuous phase while pressure would be maximum at the edges. Horizontal velocity component of droplets is recognized by the continuous phase velocity which indicates droplets are dragged by the continuous phase flow. On the other hand, vertical component of droplet velocity strongly depends on the control parameters like droplet size, droplet distance, initial configuration, relative orientation of droplets, capillary number. We have found that the vertical velocity profile of droplets increases monotonically from zero where all droplets are flowing on center line of channel, to its maximum value. After that, the vertical velocity component decreases by increasing the relative orientation of droplets. On the other hand, perturbation created in the continuous flow is a result of droplet moving through the channel. It has been found that deformable and rigid droplets display different collective dynamics. Rigid droplets do not drift normal to the channel walls and therefore the vertical component of their velocity is approximately zero. While, as the capillary number increases, deformable drops tend to approach more to the center of the channel at which the pressure is maximum. The vertical velocity component of droplet strongly depends on the droplet size. It increases by increasing the droplet size. Viscosity ratio and capillary number are other parameters influencing the control of the system. By knowing the effects and behaviors of these parameters, they can be controlled and manipulated over their application. Our results play an important role in estimating the necessary time to obtain the self-assembly.

The droplet migration could also be relevant for other systems such as blood microcirculation. In blood microcirculation, for instance it may play a key role in the segregation of flowing blood phenomenon that could lead to red blood cell aggregation [43].

Acknowledgments Kadivar acknowledges the support of Shiraz University of Technology Research Council.

Author Contributions EK designed the research and developed the simulation code. MF and FG ran the simulations. EK analyzed and interpreted the results and wrote the manuscript.

Compliance with Ethical Standards

Conflict of interest The authors declare that they have no conflicts of interest.

References

1. N.T. Nguyen, S. Wereley, *Fundamentals and Applications of Microfluidics* (Artech House, Boston, 2002)

2. N.T. Nguyen, Micro-magnetofluidics: interactions between magnetism and fluid flow on the microscale. Microfluid. Nanofluid. **12**, 1 (2012)
3. S. Hutzler, N. Peron, D. Weaire, W. drenckhan, The foam/emulsion analogy in structure and drainage. Eur. Phys. J. E **14**, 381 (2004)
4. C. Priest, S. Herminghaus, R. Seemann, Controlled electrocoalescence in microfluidics: targeting a single lamella. Appl. Phys. Lett. **88**, 024106 (2006)
5. J. Sivasamy, Y.C. Chim, T.N. Wong, N.T. Nguyen, L. Yobas, Reliable addition of reagents into microfluidic droplets. Microfluid. Nanofluid. **8**, 409 (2010)
6. L.G. Leal, Particle motions in a viscous fluid. Ann. Rev. Fluid Mech. **12**, 435 (1980)
7. P.C.H. Chan, L.G. Leal, The motion of a deformable drop in a second-order fluid. J. Fluid Mech. **92**, 131 (1979)
8. J.A. Stoos, S.M. Yang, L.G. Leal, Hydrodynamic interaction of a small fluid particle and a spherical drop in low-Reynolds number flow. Int. J. Multiphase Flow **18**, 1019 (1992)
9. J. Bibette, D. Morse, T. Witten, D.A. Weitz, Stability criteria for emulsions. Phys. Rev. Lett. **69**, 2439 (1992)
10. J. Bibette, F.L. Calderon, P. Poulin, Emulsions: basic principles. Rep. Prog. Phys. **62**, 696 (1999)
11. J.C. Baret, Surfactants in droplet-based microfluidics. Lab Chip **12**, 422 (2012)
12. J.C. Baret, F. Kleinschmidt, A.E. Harrak, A.D. Griffith, Kinetic aspects of emulsion stabilization by surfactants: a microfluidic analysis. Langmuir **25**, 6088 (2009)
13. M.K. Lyon, L.G. Leal, An experimental study of the motion of concentrated suspensions in two-dimensional channel flow. Part 2. Bidisperse systems. J. Fluid Mech. **363**, 57 (1998)
14. S. Mortazavi, G. Tryggvason, A numerical study of the motion of drops in Poiseuille flow. Part 1. Lateral migration of one drop. J. Fluid Mech. **411**, 325 (2000)
15. E. Kadivar, M. Farrokhbin, Phys. A **479**, 449 (2017)
16. E. Kadivar, A. Alizadeh, Eur. Phys. J. E **40**, 31 (2017)
17. H.L. Goldsmith, S.G. Mason, The flow of suspensions through tubes. I. Single spheres, rods, and discs. J. Colloid Sci. **17**, 448 (1962)
18. P.C.H. Chan, L.G. Leal, An experimental study of drop migration in shear flow between concentric cylinders. Int. J. Multiphase Flow **7**, 83 (1981)
19. J.R. Smart, D.T. Leighton, Measurement of the drift of a droplet due to the presence of a plane. Phys. Fluids A **3**, 21 (1991)
20. E. Kadivar, Droplet trajectories in a flat microfluidic network. Eur. J. Mech. B. Fluids **57**, 75 (2016)
21. M. Seo, Z. Nie, S. Xu, P.C. Lewis, E. Kumacheva, Microfluidics: from dynamic lattices to periodic arrays of polymer disks. Langmuir **21**, 4773 (2005)
22. J.P. Raven, P. Marmottant, Periodic microfluidic bubbling oscillator: insight into the stability of two-phase microflows. Phys. Rev. Lett. **97**, 154501 (2006)
23. R. Mehrotra, N. Jing, J. Kameoka, Monodispersed polygonal water droplets in microchannel. Appl. Phys. Lett. **92**, 213109 (2008)
24. P. Marmottant, J.P. Raven, Microfluidics with foams. Soft Matter **5**, 3385 (2009)
25. N. Kern, D. Weaire, A. Martin, S. Hutzler, S.J. Cox, Two-dimensional viscous froth model for foam dynamics. Phys. Rev. E **70**, 041411 (2004)
26. P. Garstecki, Whitesides GM Tessellation of a stripe. Phys. Rev. E **73**, 031603 (2006)
27. E. Kadivar, Quasistatic packings of droplets in flat microfluidic channels. Phys. A **443**, 486 (2016)
28. T. Beatus, T. Tlusty, R.B. Ziv, Phonons in a one-dimensional microfluidic crystal. Nat. Phys. **2**, 743 (2006)
29. T. Beatus, T. Tlusty, R.B. Ziv, Burgers shock waves and sound in a 2d microfluidic droplets ensemble. Phys. Rev. Lett. **103**, 114502 (2009)
30. M. Loewenberg, E.J. Hinch, Collision of two deformable drops in shear flow. J. Fluid Mech. **338**, 299 (1997)
31. K.G. Hollingsworth, M.L. Johns, Droplet migration in emulsion systems measured using MR methods. J. Colloid Interface Sci. **296**, 700 (2006)
32. X. Li, H. Zhou, C. Pozrikidis, A numerical study of the shearing motion of emulsions and foams. J. Fluid Mech. **286**, 379404 (1995)
33. P.J.A. Janssen, M.D. Baron, P.D. Anderson, J. Blawzdziewicz, M. Loewenberg, E. Wajnryb, Collective dynamics of confined rigid spheres and deformable drops. Soft Matter **8**, 7495 (2012)
34. J.B. Fleury, U.D. Schiller, S. Thutupalli, G. Gompper, R. Seemann, Mode coupling of phonons in a dense one-dimensional microfluidic crystal. New J. Phys. **16**, 063029 (2014)
35. K.V. McCloud, J.V. Maher, Experimental perturbations to Saffman-Taylor flow. Phys. Rep. **260**, 139 (1995)
36. C. Liu, Z. Li, On the validity of the Navier-Stokes equations for nanoscale liquid flows: The role of channel size. AIP Adv. **1**, 032108 (2011)
37. C.W. Park, M. Homsy, Two-phase displacement in hele shaw cells: theory. J. Fluid Mech. **139**, 291 (1984)
38. C. Pozrikids, *A Practical Guide to Boundary Element Methods* (CRC Press, Florida, 2002)
39. T. Dessup, T. Maimbourg, C. Coste, M.S. Jean, Linear instability of a zigzag pattern. Phys. Rev. E **91**, 022908 (2015)
40. E. Kadivar, S. Herminghaus, M. Brinkmann, Droplet sorting in a loop of flat microfluidic channels. J. Phys. Condens. Matter **25**, 285102 (2013)
41. R. Mehrotra, Monodispersed polygonal water droplets in microchannel, Texas A&M University (2008)
42. A. Karins, S. Mason, Particle motions in sheared suspensions: XXIII. Wall migration of fluid drops. J. Colloid Interface Sci. **24**, 164 (1967)
43. B. Kaoui, T. Krüger, J. Harting, How does confinement affect the dynamics of viscous vesicles and red blood cells? Soft Matter **8**, 9246 (2012)